ISSN 1070-3284, Russian Journal of Coordination Chemistry, 2023, Vol. 49, No. 5, pp. 257–266. © Pleiades Publishing, Ltd., 2023.
Russian Text © The Author(s), 2023, published in Koordinatsionnaya Khimiya, 2023, Vol. 49, No. 5, pp. 259–268.

The First Perylene Complexes of Neodymium and Dysprosium

T. V. Balashova[a], *, S. K. Polyakova[a], A. A. Fagin[a], V. A. Ilichev[a], K. A. Kozhanov[a], E. V. Baranov[a], G. K. Fukin[a], and M. N. Bochkarev[a]

[a] *Razuvaev Institute of Organometallic Chemistry, Russian Academy of Sciences, Nizhny Novgorod, Russia*

**e-mail: petrovsk@iomc.ras.ru*

Received July 8, 2022; revised September 9, 2022; accepted September 14, 2022

Abstract—Neodymium and dysprosium perylene complexes $LnI(Per)(DME)_2 \cdot Per$ (Ln = Nd, Dy) were obtained for the first time by the reaction of the Ln diiodides with perylene in dimethoxyethane. The structure of dysprosium complex was established by X-ray diffraction (CCDC no. 2184200). Experimental–theoretical electron density analysis was performed to specify the type of coordination between the dysprosium cation and perylene in $DyI(Per)(DME)_2 \cdot Per$. Despite the identical composition, the Nd and Dy complexes have different structures, which is reflected in their luminescence properties.

Keywords: neodymium, dysprosium, perylene, X-ray diffraction, photoluminescence, experimental–theoretical electron density analysis

DOI: 10.1134/S1070328423700471

INTRODUCTION

Polycyclic aromatic hydrocarbons (PAHs) attract the attention of researchers due to a number of unique properties. Owing to the planarity of molecules and the extended system of conjugated π-bonds, they are effective donor components in donor-accepror materials both in the solid state and in solutions [1–3]. Good optoelectronic properties make PAHs applicable in advanced fields of photonics and electronics as materials for organic light-emitting diodes (OLEDs), field-effect transistors, and photovoltaic cells [4–8]. PAHs can also serve as synthetic precursors for the synthesis of fullerenes, carbon nanotubes, nanographene and so on [9]. In recent years, the interest in the development of new materials based on perylene chromophores has been revived because of their exceptional chemical and photochemical stability [10], high fluorescence quantum yields [11], and the broad range of colors available via introduction of substituents into the perylene core [12]. Currently, most studies in this field are devoted to readily available perylene tetracarboximides [13–15], perylenetetracarboxylic acid, and its anhydride [16–18], in which metal atoms are linked to the perylene ligands via functional groups. A few papers also describe compounds in which the metal atom is π-bonded directly to the perylene core [19–23]. The metal compounds in which the metal is σ-bonded to the aromatic perylene core have been little studied. Most of these compounds contain transition metals (Pd, Pt) and are obtained from bromo-substituted perylene derivatives [24, 25]. Organometallic lanthanide compounds with perylene ligands had not been obtained by the beginning of our studies.

EXPERIMENTAL

The synthesis was carried out under conditions ruling out the contact with air oxygen and moisture using the standard Schlenk technique. Dimethoxyethane (DME) was dried with sodium benzophenone ketyl by a standard procedure and withdrawn in vacuum immediately prior to use. TmI_2, NdI_2, and DyI_2 were obtained by known procedures [26, 27]. Elemental analysis for C and H was carried out on an Elementar Vario ELcube analyzer. Because of the exceptional instability of the obtained organolanthanide compounds in air, the data of C, H elemental analysis were poorly reproducible. Therefore, the compounds were analyzed only for metal and iodine by complexometric titration. IR spectra were recorded on an FSM-1201 FTIR spectrometer in the 4000–400 cm^{-1} range. The samples were prepared as mineral oil mulls. The absorption spectra were measured in a 1-cm quartz cell on a PerkinElmer Lambda-25 spectrometer in the range from 200 to 700 nm. Photoluminescence (PL) spectra were recorded on a USB2000 spectrometer on excitation with a diode laser at 405 nm. ESR spectra were run on a Bruker Magnettech MS5000 spectrometer equipped with a standard cavity and operating at ~9.5 GHz. The magnetic moments were measured at room temperature on an instrument manufactured in the laboratory, based on the Faraday method, using comparison with known samples, as described earlier [28]. The error of measurements did not exceed 5%.

Synthesis of DyI(Per)(DME)$_2$·Per (I). DME (15 mL) was recondensed into a mixture of perylene (0.0273 g, 0.11 mmol) and DyI_2 (0.090 g, 0.26 mmol) powders. As the reaction mixture was continuously stirred and heated from −45 to −10°C, the solution gradually acquired a violet-burgundy color. After the mixture was kept for 2 h at −10°C, $DyI_3(DME)_3$ precipitated as a light gray solid. The solution was decanted from the precipitate, which was washed with cold DME and dried in vacuum. The yield was 70 mg (89%).

The solution was concentrated to half of the volume. On cooling down to −20°C, a small amount of crystals suitable for X-ray diffraction precipitated. The crystals were separated by decantation, washed with cold DME, and dried in vacuum. The solvent was completely removed from the solution, the remaining dark burgundy-colored solid was washed with cold DME and dried. The yield was 67 mg (63%).

For $C_{48}H_{44}O_4IDy$		
Anal. calcd., %	Dy, 16.68	I, 13.03
Found, %	Dy, 16.37	I, 13.61

IR (KBr; ν, cm^{-1}): 1282 m, 1249 w, 1237 m, 1206 w, 1187 m, 1153 w, 1111 m, 1083 m, 1068 s, 1023 s, 969 m, 850 s, 826 s, 809 s, 572 w, 556 m, 462 m.

Synthesis of NdI(Per)(DME)$_2$·Per (II) was carried out similarly to **I** starting from perylene (34 mg, 0.13 mmol) and NdI_2 (107 mg, 0.27 mmol) in DME. The yield was 76 mg (61%).

For $C_{48}H_{44}O_4INd$		
Anal. calcd., %	Nd, 15.09	I, 13.27
Found, %	Nd, 15.34	I, 13.55

The IR spectrum of complex **II** was similar to the spectrum of **I**.

X-ray diffraction study of I was carried out on a Bruker D8 Quest automated diffractometer (MoK_α radiation, φ- and ω-scan mode, λ = 0.71073 Å). Collection of diffraction data, initial reflection indexing, and refinement of unit cell parameters were performed using the APEX3 software [29]. The experimental sets of intensities were integrated using the SAINT software [30, 31]. The SADABS program [32] was used to apply absorption corrections. The structure was solved by the direct methods with the dual-space algorithm in the SHELXT program [33]. The non-hydrogen atoms were refined by full-matrix least-squares on F^2_{hkl} in the anisotropic approximation using the SHELXTL program package [34, 35]. The hydrogen atoms, except for H(1) and H(20), were placed in the geometrically calculated positions and refined in the riding model ($U_{iso}(H) = 1.5U_{equiv}(C)$ for the CH_3 groups, $U_{iso}(H) = 1.2U_{equiv}(C)$ for other groups). The H(1) and H(20) atoms were located from the difference Fourier electron density maps and refined in the isotropic approximation. The crystal of **I** was found to contain non-coordinated perylene molecules in 1 : 1 ratio to Dy. The main crystallographic characteristics and X-ray diffraction experiment details for **I** are summarized in Table 1, and selected bond lengths and angles are in Table 2.

Additional crystallographic data for **I** was deposited with the Cambridge Crystallographic Data Centre (CCDC no. 2184200; http://ccdc.cam.ac.uk/structures/).

Crystal invariom for complex I. Single-point DFT calculations for the periodic 3D structure of DyI(Per)(DME)$_2$·Per (**I**) were carried out with the B3LYP exchange correlation functional [36, 37] in the CRYSTAL17 program [38] using a mixed all-electron basis set representing modified DZP with missed *g*-functions for Dy [39] and I [40] atoms, and 6-31G(d,p) basis set for C, O [41, 42] and H atoms [42, 43]. The atom coordinates for the single-point DFT calculations were taken from the data of the routine X-ray diffraction experiment for **I**. The compression ratio of the inverse space was set to be four, which corresponds to 30 K points in the irreducible Brillouin zone in which the Hamiltonian matrix was diagonalized.

The PLATON program (version 60119) [44] was used to generate 49621 independent *hkl* Miller indices with inverse resolution of up to $s = 1.16$ Å^{-1}. The XFAC option of the CRYSTAL17 program was used to obtain a set of theoretical structural factors F_{hkl} from the electron density function derived from single-point calculations of the non-optimized crystal structure of **I**.

Using the calculated structural amplitudes F_{hkl}, the populations of the spherically symmetric valence shell (P_{val}) and the multipole parameters (P_{lm}) describing shell deformation, together with the corresponding expansion–compression ratios (k, k') were found for each atom of **I** using the MoPro program [45] in the framework of the Hansen–Coppens multipole density formalism [46]. Before the multipole refinement, the C–H bond lengths were normalized to the values found in the neutron diffraction experiments [47]. The levels of the multipole expansions were hexadecapole for dysprosium and iodine atoms, octupole for all other non-hydrogen atoms, and one dipole for hydrogen atoms. The obtained P_{val}, P_{lm}, k, and k' values were used for the multipole refinement (but were not refined themselves) of the atom coordinates and thermal parameters for complex **I** using experimental reflections ($\sin\theta/\lambda = 0.64$ Å^{-1}) in the real crystal symmetry.

The topology of the experimental–theoretical function ρ(**r**) was analyzed using the WINXPRO program package [48].

Table 1. Crystallographic data and X-ray experiment and structure refinement details for **I**

Characteristics	Value
Molecular formula	$C_{48}H_{44}O_4IDy$
M	974.23
Temperature, K	100(2)
System	Monoclinic
Space group	$P2_1/n$
a, Å	11.0917(6)
b, Å	26.1845(15)
c, Å	13.4206(8)
β, deg	103.318(2)
V, Å^3	3792.9(4)
Z	4
ρ(calcd.), mg/cm^3	1.706
μ, mm^{-1}	2.830
Crystal size, mm	0.31 × 0.27 × 0.07
F(000)	1932
Data collection range of 2θ, deg	2.20–27.00
Number of reflections collected/unique	97 162/8262
R_{int}	0.1258
R_1 ($I > 2\sigma(I)$)	0.0680
wR_2 ($I > 2\sigma(I)$)	0.0998
R_1 (for all data)	0.0906
wR_2 (for all data)	0.1042
S	1.236
Residual electron density (max/min), e/Å^3	1.458/–2.294

RESULTS AND DISCUSSION

Earlier studies of the reaction of low-oxidation-state lanthanide diiodides LnI_2 (Ln = Tm, Dy, Nd) showed that, in conformoty with the high Tm^{2+} reduction potential (–2.3 V) [49], thulium diiodide does not reduce naphthalene in the direct reaction in ether solvents. As indicated by comparison of the electrode potentials of Tm, Dy, and Nd ($E_o(Ln^{3+}/Ln^{2+})$ of –2.3, –2.45, and –2.62 V, respectively) [49], the reducing properties of divalent metal iodides markedly increase on going from thulium to dysprosium and neodymium [50]. The reactions of NdI_2 with polycyclic aromatic compounds such as naphthalene and anthracene give the binuclear complexes $[NdI_2(THF)_3]_2(C_{10}H_8)$ and $[NdI_2(THF)_3]_2(C_{14}H_{10})$ containing the arene dianion [50]. The reactions of NdI_2 and DyI_2 with perylene in DME proceed in a different way. Presumably, the reactions involve the formation of an intermediate product containing one $[LnI_2]^+$ moiety and the perylene radical anion ($Per^{\cdot-}$) (Scheme 1), as evidenced by the blue color of the solution and the ESR signal, which disappears in a few minutes, and the reaction mixture becomes dark burgundy colored. The ESR spectrum of the hypothesized intermediate $[LnI_2(Per^{\cdot-})(DME)_2]$ at room temperature (Fig. 1) is a singlet with $g_i = 2.0038$ and a line width of ~12 Oe.

The subsequent transformations afford mononuclear compounds $LnI(Per)(DME)_2$, containing the perylene dianion, and the triiodides $LnI_3(DME)_2$, resulting from disproportionation (Scheme 1). Disproportionation reactions in the presence of organic substrates are characteristic of neodymium and dysprosium diiodides [50, 51].

Table 2. Selected bond lengths and bond angles in complex **I**

Bond	*d*, Å	Bond	*d*, Å
Dy(1)–I(1)	3.0941(5)	Dy(1)–C(11)	2.638(6)
Dy(1)–O(1)	2.413(4)	Dy(1)–C(20)	2.529(7)
Dy(1)–O(2)	2.406(4)	C(1)–C(2)	1.418(10)
Dy(1)–O(3)	2.458(4)	C(1)–C(10)	1.445(9)
Dy(1)–O(4)	2.465(5)	C(10)–C(11)	1.410(9)
Dy(1)–C(1)	2.584(7)	C(11)–C(20)	1.457(9)
Dy(1)–C(10)	2.686(6)	C(19)–C(20)	1.403(10)
Angle	ω, deg	Angle	ω, deg
O(1)Dy(1)O(2)	67.40(16)	I(1)Dy(1)C(10)	135.31(15)
O(2)Dy(1)O(3)	140.86(15)	I(1)Dy(1)C(11)	163.13(15)
O(3)Dy(1)O(4)	67.56(15)	I(1)Dy(1)C(20)	163.87(15)
O(4)Dy(1)O(1)	76.20(16)	I(1)Dy(1)O(1)	94.69(11)
O(1)Dy(1)O(3)	143.34(16)	I(1)Dy(1)O(2)	77.43(11)
O(2)Dy(1)O(4)	137.03(16)	I(1)Dy(1)O(3)	76.54(11)
C(1)Dy(1)C(10)	31.76(19)	I(1)Dy(1)O(4)	83.78(11)
C(10)Dy(1)C(11)	30.7(2)	I(1)Dy(1)C(1)	115.43(16)
C(11)Dy(1)C(20)	32.7(2)	I(1)Dy(1)C(10)	135.31(15)
C(1)Dy(1)C(20)	69.6(2)	I(1)Dy(1)C(11)	163.13(15)
I(1)Dy(1)C(1)	115.43(16)	I(1)Dy(1)C(20)	163.87(15)

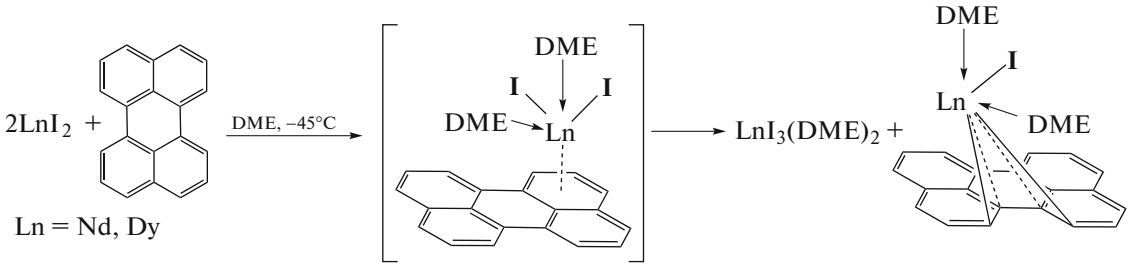

Scheme 1.

A similar reaction pathway was observed in the reaction of DyI_2 with naphthalene in DME [52].

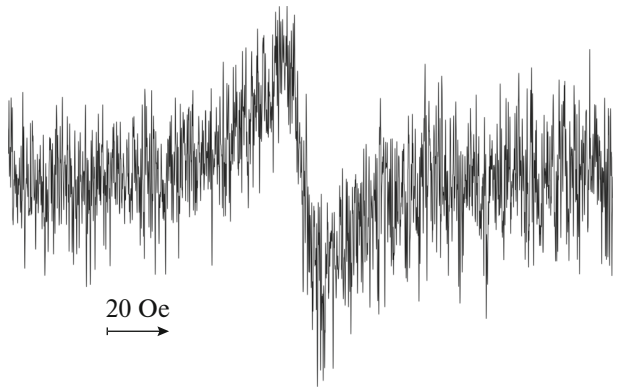

Fig. 1. ESR spectrum of the reaction mixture (DyI_2 + Per) in DME at 290 K.

Complex **I** was isolated as dark violet crystals in 60% yield. The compound was extremely sensitive to air oxygen and moisture and immediately decomposed to give free perylene.

The perylene ligand in **I** occurs as the dianion, as indicated by the absence of the ESR signal both in solution and in the solid state. The molecular structure of $DyI(Per)(DME)_2$ was determined by X-ray diffraction (Fig. 2).

The Dy(1) atom is coordinated by the perylene ligand, iodine atom, and additionally by two neutral DME molecules. The coordination number of dysprosium is 8. The perylene ligand is coordinated to Dy(1) via four carbon atoms, C(1), C(10), C(11), and C(20), with all its protons being retained, including H(1) and H(20). The peripheral Dy(1)–C(1) and Dy(1)–C(20) metal–perylene bonds (2.584(7), 2.529(7) Å) are shorter than the internal Dy(1)–C(10)

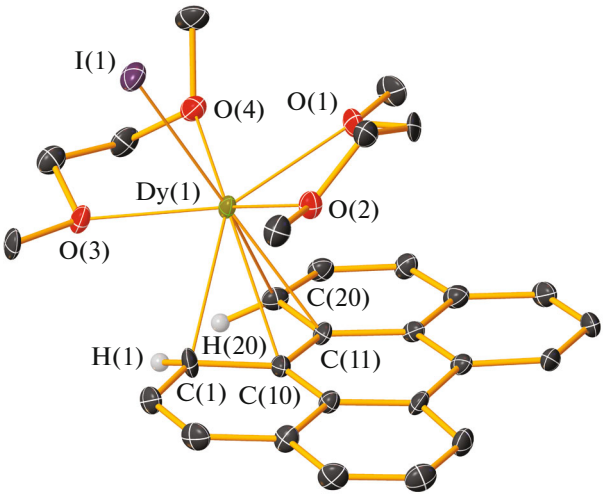

Fig. 2. Molecular structure of the complex $DyI(Per)(DME)_2$. The thermal ellipsoids are shown at 50% probability level. The hydrogen atoms, except for H(1) and H(20), are omitted.

and Dy(1)–C(11) bonds (2.686(6), 2.638(6) Å). Note that the Dy(1)–C(10, 11) distances are smaller than the sum of the Dy^{3+} ionic radius (1.027 Å with C.N. of 8 [53]) and the van der Waals radius of carbon (1.7 Å [54]), which is 2.727 Å. Apart from the $DyI(Per)(DME)_2$ molecule, the asymmetric part of the crystal cell was found to contain a non-coordinated perylene molecule, which exists in the neutral form, as indicated by the C–C bond lengths (Fig. 3a). Analysis of the perylene ligand geometry indicates that the most pronounced changes in the C–C bond lengths in comparison with non-coordinated Per take place in the coordinated part of the Per ligand (between the C(1)–C(10), C(10)–C(11), and C(11)–C(20) atoms) (Figs. 3a and 3b).

In the perylene ligand, the C(1)–C(10) and C(11)–C(20) bonds are elongated, but the C(10)–C(11) bond is shortened with respect to analogous bonds in neutral perylene (Fig. 3a). The coordination of the perylene dianion to dysprosium does not result in equalization of C–C distances in the Dy(1)C(1)C(10)C(11)C(20) ring. The C(1)–C(10), C(10)–C(11), and C(11)–C(20) bond lengths alternate. According to the formal double and single bond distribution in the perylene ligand, the negative charges of the perylene dianion are localized on the C(1) and C(20) atoms (Fig. 3b). Apart from two electron pairs of the C(1) and C(20) atoms, the electron pair of the C(10)–C(11) bond additionally participates

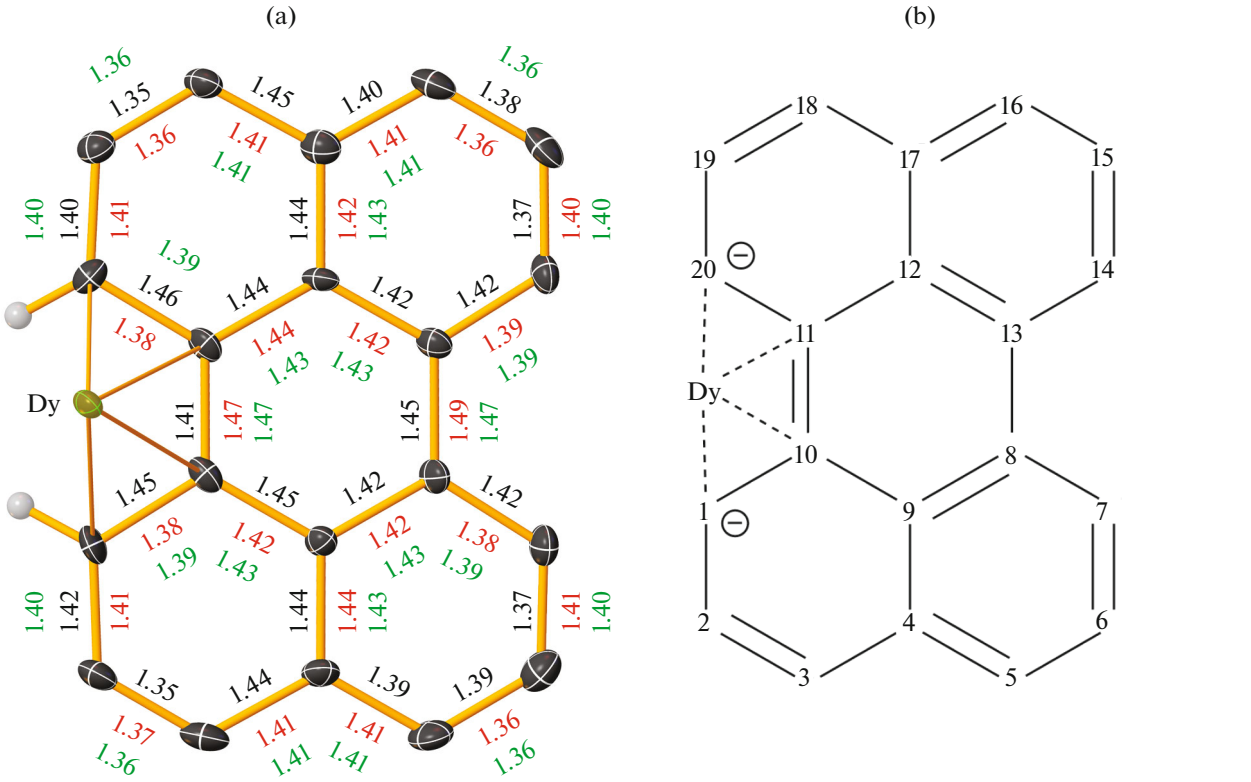

Fig. 3. (a) Lengths of the C–C bonds in the Per ligand (black digits) and analogous bond lengths for non-coordinated Per (red digits). Green digits indicate the average C–C distances in the perylene molecules according to CCDC [55]; (b) carbon atom numbering and formal double and single bond distribution scheme in the perylene dianion according to the X-ray diffraction data.

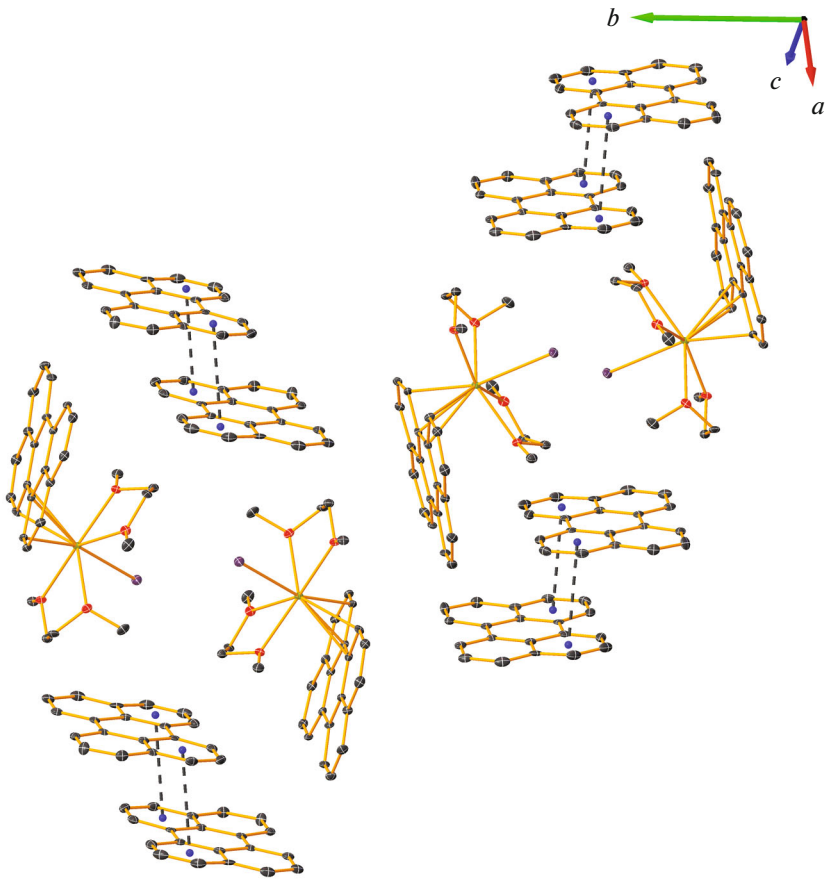

Fig. 4. Fragment of the crystal packing of complex **I**.

in the Per coordination to Dy; hence, the coordination number of the perylene dianion is three [56].

It is noteworthy that the neutral and dianionic perylenes are planar, the deviations of carbon atoms from the perylene plane differ insignificantly (0.036 and 0.078 Å, respectively).

In the coordinated part of the perylene ligand, the H(1) and H(20) atoms deviate from the perylene plane away from the Dy atom by 0.20 and 0.41 Å, respectively. The average value for similar hydrogen atoms in non-coordinated perylene is 0.06 Å.

In the crystal packing of complex **I**, π-stacking of neutral perylene molecules in pairs takes place (Fig. 4). In the π–π interaction, the perylene molecules overlap by pairs of benzene rings with a minor displacement; the distance between the ring centers is 3.52 Å. This value falls in the range of distances characteristic of π–π interactions (3.3–3.8 Å [57]) and is close to the sum of the van der Waals radii of carbon atoms (3.4 Å [54]). The interplanar spacing between the perylene molecules involved in the π stacking is 3.29 Å.

Although the Dy(1)–C(10, 11) coordination bonds are markedly elongated compared to the Dy(1)–C(1, 20) distances (Fig. 2), but do not exceed the sum of the Dy^{3+} ionic radius and the carbon van der Waals radius (2.727 Å), we decided to find out, in the most correct way, which type of coordination (η^2 or η^4) exists between the dysprosium cation and the perylene dianion. For this purpose, we used analysis of the experimental–theoretical electron density ($\rho(\mathbf{r})$) for complex **I**, based on the aspherical scattering factor of the independent part of the unit cell (crystal invariom). Previously, we showed that the crystal invariom adequately describes the experimental topological characteristics $\rho(\mathbf{r})$ in the chromium coordination sphere [58]. Using R. Bader's theory [59], we constructed the experimental–theoretical molecular graph of complex **I** (Fig. 5).

According to the molecular graph, bond paths and critical points (CPs) (3, –1) are present between the Dy(1) and C(1) and C(20) atoms. Hence, there are interatomic interactions between these atoms. Meanwhile, no bond paths and CP(3, –1) are detected between Dy(1) and C(10) or C(11). In terms of R. Bader's theory, this can be interpreted as the absence of interatomic interactions. However, there are numerous examples of interactions of metal atoms with π-carbocyclic systems in which the number of bond paths between the metal and the ligand is smaller

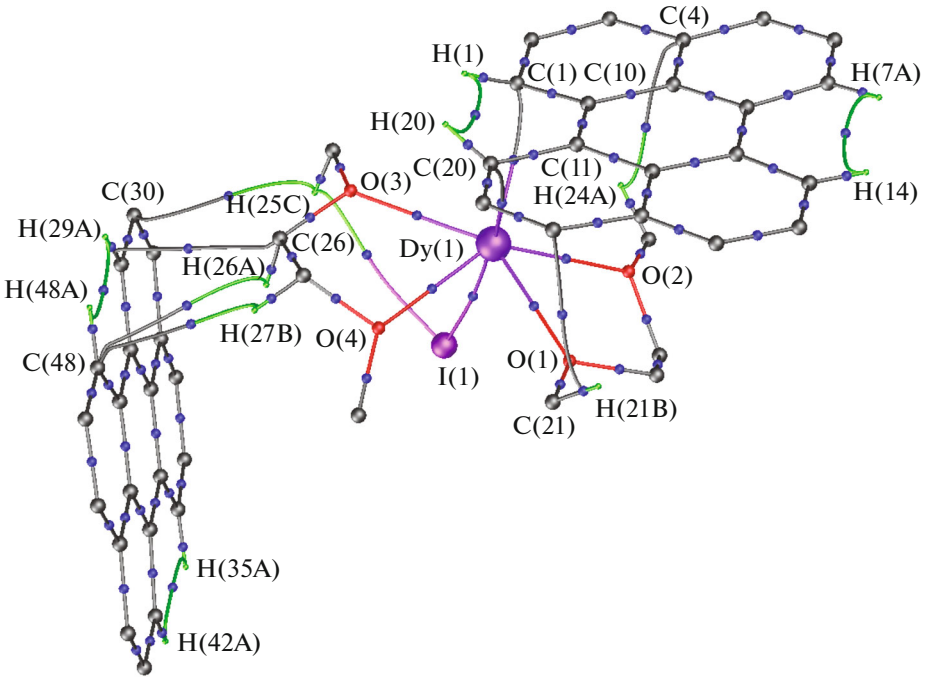

Fig. 5. Molecular graph in the independent part of the unit cell of complex **I**. The blue points correspond to the (3, –1) critical points.

than expected [60–62]. This is usually due to low curvature of the electron density. In order to assess the presence of interatomic interactions in the absence of bond paths and CP(3, –1) in these systems, we resorted to an approach [62] based on the simultaneous use of the source function (SF) [63–65] and non-covalent interaction index (NCI) [66–68]. The values for the source function for the Dy(1)C(1)C(10)C(11)C(20) moiety to the chosen reference points are given in Table 3. As can be seen from Table 3, the Dy atoms are electron density sources for interaction with the C(1)C(10)C(11)C(20) moiety. In turn, each carbon atom (given in bold in Table 3) in the C(1)C(10)C(11)C(20) moiety is an electron density source for the interaction with Dy(1). Hence, η^4-interaction is implemented between the dysprosium cation and perylene. The Dy(1)–I(1) and Dy(1)–O(1–4) contacts are ionic (i.e., closed-shell interactions; $\nabla^2\rho(\mathbf{r}) > 0$, $h_e(\mathbf{r}) > 0$), while the Dy(1)–C(1, 20) contacts are intermediate (polar covalent bonds; $\nabla^2\rho(\mathbf{r}) > 0$, $h_e(\mathbf{r}) < 0$).

The magnetic moments of the Nd and Dy complexes (3.1 and 10 μ_B, respectively) are in the range typical of organic compounds of these metals in the

Table 3. Contribution of the source function to the chosen reference point

Reference points	Source function, %				
	Dy(1)	C(1)	C(10)	C(11)	C(20)
$[Dy(1)–C(1)]_{CP(3, -1)}$[a]	**16.8**	–18.2	**4.6**[d]	**3.2**	**8.1**
$[Dy(1)–C(20)]_{CP(3, -1)}$	**19.8**	–0.9	**3.4**	**4.4**	–7.1
$[Dy(1)–C(10)]_{middle}$[b]	**18.6**	**0.2**	–20.1	**1.9**	**9.8**
$[Dy(1)–C(11)]_{middle}$	**52.2**	–0.2	–0.2	–9.5	**3.8**
$[Dy(1)–C(10)]_{NCI}$[c]	**17.6**	**1.2**	**3.8**	–22.1	**10.9**
$[Dy(1)–C(11)]_{NCI}$	**17.6**	–8.4	–10.4	**4.4**	**8.9**

[a] Source function values at CP(3, –1) in the Dy(1)–C(1, 20) bonds from the Dy(1)C(1)C(10)C(11)C(20) moiety.
[b] Source function values at the center of the Dy(1)–C(10, 11) distance from the Dy(1)C(1)C(10)C(11)C(20) moiety.
[c] Source function values on the NCI isosurface between Dy(1) and C(10, 11) from the Dy(1)C(1)C(10)C(11)C(20) moiety.
[d] Positive values are the sources of electron density (donor), negative values are the electron density drain (acceptor).

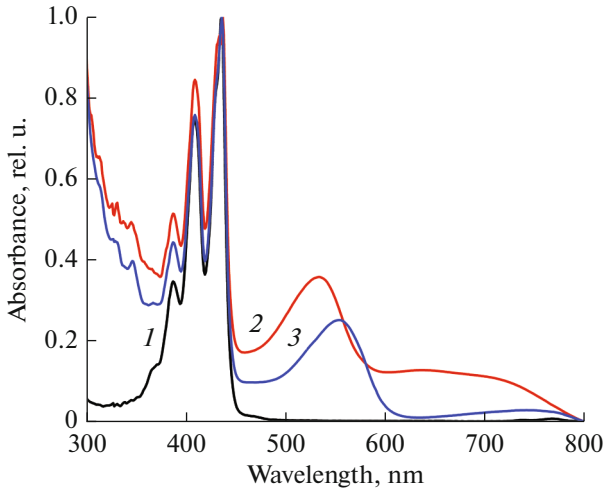

Fig. 6. Absorption spectra of (*1*) perylene and (*2*) Dy and (*3*) Nd complexes in DME solution (10^{-5} M).

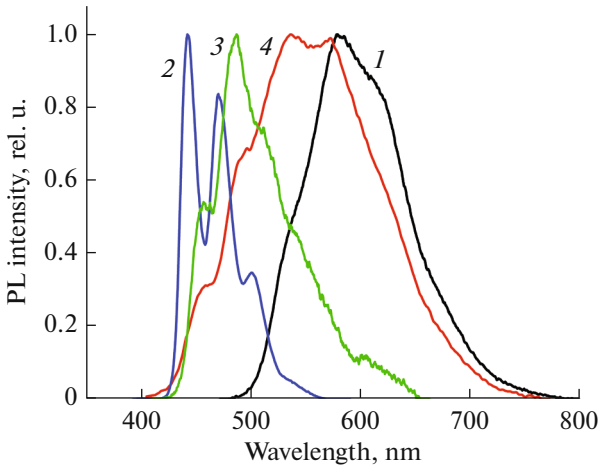

Fig. 7. PL spectra of a solid sample of (*1*) perylene, (*2*) perylene in DME solution (10^{-5} M), and solid samples of (*3*) Nd complex and (*4*) Dy complex, λ_{excit} = 405 nm at room temperature.

trivalent state (Nd, 2.98–3.7; and Dy, 9.9–10.6 μ_B) [69].

An X-ray diffraction study of neodymium complex **II** could not be performed, but the preparation method, the contents of neodymium and iodine, the IR spectrum, magnetic moment, and the absence of ESR spectrum suggest that its composition and structure are similar to those of complex **I**.

Thulium diiodide TmI_2 does not react with perylene (like with naphthalene) in DME not only at low temperature, but also under more drastic conditions (30°C in an ultrasonic bath).

The absorption spectra of complexes **I** and **II** in DME at room temperature are superpositions of the absorption of neutral perylene, which is always present in the complexes, and the absorption of the lanthanide coordination compound containing doubly reduced perylene (Fig. 6). Apart from the intense sharp bands at 409 and 436 nm and the band at 387 nm, corresponding to the π–π* transitions in neutral perylene, the spectrum exhibits intense broad bands with a maximum at 533 nm (Dy) and 555 nm (Nd) and less intense bands in the 600–800 nm range, which should be assigned to electronic transitions within the complexes.

Compounds **I** and **II** exhibit photoluminescence (PL) in the solid state.

The fluorescence spectra of a solid sample of free perylene, its dilute DME solution, and solid samples of the neodymium and dysprosium complexes are shown in Fig. 7. The PL spectrum of a dilute perylene solution in DME shows a vibrational structure of four peaks at 442, 470, 500, and 550 nm, which can be assigned to the perylene solvation molecule [70]. It is known that perylene crystals have a stable α-phase, which is dimeric, and the metastable β-phase, which is monomeric, with their emission maxima being at 600 and 520 nm, respectively [71]. The spectrum of a solid perylene sample, shown in Fig. 7, with a maximum at 580 nm and a shoulder at 614 nm can be assigned to α-phase fluorescence. The fluorescence of polycyclic aromatic hydrocarbons is strongly affected by the local spatial environment. Although the composition is the same, the luminescence spectra of neodymium and dysprosium complexes are significantly different (Fig. 7). The PL spectrum of a solid sample of the Nd complex has an emission maximum at 490 nm.

The PL spectrum of the Dy complex exhibits a broad band with two maxima at 536 and 573 nm. It is known that the polycyclic aromatic compounds such as pyrene and α-perylene may give rise to Y and E type excimer emission [72] in the solid state under normal conditions [73] with λ_{em} at about 560–590 nm [70]. The appearance of excimer fluorescence is related to the structural features of the compounds, namely, the formation of pairs in which short contacts and π–π stacking between neighboring molecules are present [74].

Consequently, the luminescence properties of the Nd and Dy perylene complexes may be caused by the luminescence of the perylene molecules contained in the crystal in different chemical environments. This assumption is also supported by the absence of any PL of compounds **I** and **II** in DME solutions (except for PL of perylene) and by the absorption of the complexes $LnI(Per)(DME)_2 \cdot Per$ in the long-wavelength region (600–800 nm).

Thus, neodymium and dysprosium diiodides are strong reducing agents capable of reducing perylene to the dianion in reactions carried out in ether solvents. The molecular structure of $DyI(Per)(DME)_2 \cdot Per$ was determined by X-ray diffraction. The perylene ligand is coordinated to dysprosium in the η^4-mode via four

carbon atoms, as was confirmed by experimental–theoretical electron density analysis. Despite the identical composition, Nd and Dy compounds demonstrate different luminescence properties. Presumably, these differences are due, first of all, to the difference of the metal local environment and crystal packing effects. By varying the crystal packing towards the formation of dimers with efficient π–π stacking, it is possible to obtain intense excimer fluorescence, which has a high potential for application as the molecular thermometer.

ACKNOWLEDGMENTS

This study was performed using the equipment of the center for collective use "Analytical Center of the Razuvaev Institute of Organometallic Chemistry, Russian Academy of Sciences" supported by the grant "Provision of the Development of the Material and Technical Infrastructure of Centers for Collective Use" (unique identifier RF–2296.61321X0017, contract number 075-15-2021-670).

FUNDING

This study was supported by the Russian Science Foundation (grant no. 22-23-00547).

CONFLICT OF INTEREST

The authors declare that they have no conflicts of interest.

REFERENCES

1. Bock, H., Seitz, W., Sievert, M., et al., *Angew. Chem., Int. Ed. Engl.*, 1996, vol. 35, p. 2244.
2. Janiak, C. and Hemling, H., *Chem. Ber.*, 1994, vol. 127, p. 1251.
3. Nakamura, Y., Tsuihiji, T., and Mita, T., *J. Am. Chem. Soc.*, 1996, vol. 118, p. 1006.
4. Feng, X., Pisula, W., and Müllen, K., *Pure Appl. Chem.*, 2009, vol. 81, p. 2203.
5. Watson, M.D., Fechtenkötter, A., and Müllen, K., *Chem. Rev.*, 2001, vol. 101, p. 1267.
6. Wu, J., Pisula, W., and Müllen, K., *Chem. Rev.*, 2007, vol. 107, p. 718.
7. Zhang, X., Xu, Z., Si, W., et al., *Nat. Commun.*, 2017, vol. 8, p. 15073.
8. Wu, D., Zhang, Y., Zhang, J., et al., *Chem. Asian J.*, 2015, vol. 10, p. 1344.
9. Narita, A., Wang, X., Feng, X., and Müllen, K., *Chem. Soc. Rev.*, 2015, vol. 44, p. 6616.
10. Feiler, L., Langhals, H., and Polborn, K., *Liebigs Ann.*, 1995, p. 1229.
11. Wasielewski, M.R., *Org. Chem.*, 2006, vol. 71, p. 5051.
12. Quante, H., Geerts, Y., and Müllen, K., *Chem. Mater.*, 1997, vol. 9, p. 495.
13. Zhao, H., Pfisher, J., and Settles, V., *J. Am. Chem. Soc.*, 2009, vol. 131, p. 15660.
14. Schmidt, R., Oh, J., and Sun, Y., *J. Am. Chem. Soc.*, 2009, vol. 131, p. 6215.
15. Hassabo, A.G., Mohamed, A.L., and Khattab, T.A., *Luminescence*, 2022, vol. 37, p. 21.
16. Martins, S.B., de Andrade, E., and Gautam, S.K., *J. Fluoresc.*, 2021, vol. 31, p. 1855.
17. Zhang, Q., Zhang, P., Li, S., et al., *Dyes Pigm.*, 2019, vol. 171, p. 107697.
18. Pereira-Andrade, E., Brum, S.M., and Policarpo, E.M.C., *Phys. Chem. Chem. Phys.*, 2020, vol. 22, p. 20744.
19. Porter, L.C., Polam, J.R., and Bodige, S., *Inorg. Chem.*, 1995, vol. 34, p. 998.
20. Shibasaki, T., Komine, N., Hirano, M., and Komiya, S., *J. Organomet. Chem.*, 2007, vol. 692, p. 2385.
21. Arrais, A., Diana, E., Gervasio, G., et al., *Eur. J. Inorg. Chem.*, 2004, p. 1505.
22. Murahashi, T., Kato, N., Uemura, T., and Kurosawa, H., *Angew. Chem., Int. Ed. Engl.*, 2007, vol. 46, p. 3509.
23. Porter, L.C., Polam, J.R., and Bodige, S., *Inorg. Chem.*, 1995, vol. 34, p. 998.
24. Lentijo, S., Miguel, J.A., and Espinet, P., *Inorg. Chem.*, 2010, vol. 49, p. 9169.
25. Weissman, H., Shirman, E., and Ben-Moshe, T., *Inorg. Chem.*, 2007, vol. 46, p. 4790.
26. Bochkarev, M.N., Fedushkin, I.L., Fagin, A.A., et al., *Angew. Chem., Int. Ed. Engl.*, 1997, vol. 36, p. 133.
27. Bochkarev, M.N. and Fagin, A.A., *Chem.-Eur. J.*, 1999, vol. 5, p. 2990.
28. Bochkarev, M.N. and Protchenko, A.P., *PTE*, 1990, no. 1, p. 194.
29. *APEX3. Bruker Molecular Analysis Research Tool. Version 2018.7-2,* Madison: Bruker AXS Inc., 2018.
30. *SAINT. Data Reduction and Correction Program. Version 8.38A*, Madison: Bruker AXS Inc., 2017.
31. Krause, L., Herbst-Irmer, R., Sheldrick, G.M., and Stalke, D., *J. Appl. Crystallogr.*, 2015, vol. 48, p. 3.
32. Sheldrick, G.M., *SADABS. Version 2016/2. Bruker/Siemens Area Detector Absorption Correction Program*, Madison: Bruker AXS Inc., 2016.
33. Sheldrick, G.M., *Acta Crystallogr., Sect. A: Cryst. Adv.*, 2015, vol. 71, p. 3.
34. Sheldrick, G.M., *Acta Crystallogr., Sect. C: Struct. Chem.,* 2015, vol. 71, p. 3.
35. Sheldrick G.M., *SHELXTL. Version 6.14. Structure Determination Software Suite*, Madison: Bruker AXS, 2003.
36. Becke, A.D., *J. Chem. Phys.*, 1993, vol. 98, p. 5648.
37. Lee, C., Yang, W., and Parr, R.G., *Phys. Rev. B*, 1988, vol. 37, p. 785.
38. Dovesi, R., Erba, A., Orlando, R., et al., *WIREs Comput. Mol. Sci.*, 2018, vol. 8, p. e1360.
39. Jorge, F.E., Martins, L.S.C., and Franco, M.L., *Chem. Phys. Lett.*, 2016, vol. 643, p. 84.
40. Barros, C.L., de Oliveira, P.J.P., Jorge, F.E., et al., *Mol. Phys.*, 2010, vol. 108, p. 1965.
41. Hehre, W.J., Ditchfield, R., and Pople, J.A., *J. Chem. Phys.*, 1972, vol. 56, p. 2257.

42. Hariharan, P.C. and Pople, J.A., *Theor. Chim. Acta*, 1973, vol. 28, p. 213.
43. Ditchfield, R., Hehre, W.J., and Pople, J.A., *J. Chem. Phys.*, 1971, vol. 54, p. 724.
44. Spek, A.L., *Acta Crystallogr., Sect. C: Struct. Chem.*, 2015, vol. 71, p. 9.
45. Jelsch, C., Guillot, B., Lagoutte, A., and Lecomte, C., *J. Appl. Crystallogr.*, 2005, vol. 38, p. 38.
46. Hansen, N.K. and Coppens, P., *Acta Crystallogr., Sect. A: Cryst. Phys., Diffr., Theor. Gen. Crystallogr.*, 1978, vol. 34, p. 909.
47. Allen, F.H., Kennard, O., Watson, D.G., et al., *J. Chem. Soc., Perkin Trans.*, 1987, vol. 2, p. S1.
48. Stash, A.I. and Tsirelson, V.G., *J. Appl. Crystallogr.*, 2014, vol. 47, p. 2086.
49. Mikheev, N.B., *Russ. J. Inorg. Chem.*, 1984, vol. 29, p. 258.
50. Bochkarev, M.N., *Coord. Chem. Rev.*, 2004, vol. 248, p. 835.
51. Bochkarev, M.N., Fagin, A.A., and Khoroshenkov, G.V., *Russ. Chem. Bull. Int. Ed.*, 2002, vol. 51, p. 1909.
52. Evans, W.J., Allen, N.T., and Ziller, J.W., *J. Am. Chem. Soc.*, 2000, vol. 122, p. 11749.
53. Shannon, R.D., *Acta Crystallogr., Sect. A: Cryst. Phys., Diffr., Theor. Gen. Crystallogr.*, 1976, vol. 32, p. 751.
54. Batsanov, S.S., *Inorg. Mater.*, 2001, vol. 37, p. 871.
55. Groom, C.R., Bruno, I.J., Lightfoot, M.P., and Ward, S.C., *Acta Crystallogr., Sect. B: Struct. Sci., Cryst. Eng. Mater.*, 2016, vol. 72, p. 171.
56. Raymond, K.N. and Eigenbrot, Ch.W., Jr., *Acc. Chem. Res.*, 1980, vol. 13, p. 276.
57. Janiack, C.J., *Dalton Trans.*, 2000, p. 3885.
58. Fukin, G.K. and Cherkasov, A.V., *Mendeleev Commun.*, 2021, vol. 31, p. 182.
59. Bader, R.F.W., *Atoms in Molecules: A Quantum Theory*, Oxford: Clarendon, 1990.
60. Farrugia, L.J., Evans, C., Lentz, D., and Roemer, M., *J. Am. Chem. Soc.*, 2009, vol. 131, p. 1251.
61. Smol'yakov, A.F., Dolgushin, F.M., Ginzburg, A.G., et al., *J. Mol. Struct.*, 2012, vol. 1014, p. 81.
62. Fukin, G.K., Cherkasov, A.V., and Rumyantcev, R.V., *Mend. Commun.*, 2019, vol. 29, p. 346.
63. Bader, R.W.F. and Gatti, C., *Chem. Phys. Lett.*, 1998, vol. 287, p. 233.
64. Farrugia, L.J. and Macchi, J., *Phys. Chem. A*, 2009, vol. 113, p. 100058.
65. Gatti, C., *Electron Density and Chemical Bonding*, Berlin: Springer, 2012, vol. 147, p. 193.
66. Johnson, E.R., Keinan, S., and Mori-Sanchez, P., *J. Am. Chem. Soc.*, 2010, vol. 132, p. 6498.
67. Contreras-Garcia, J., Johnson, E.R., and Keinan, S., *J. Chem. Theory Comput.*, 2011, vol. 7, p. 625.
68. Contreras-Garcia, J., Yang, W., and Johnson, E.R., *J. Phys. Chem. A*, 2011, vol. 115, p. 12983.
69. Evans, W.J. and Hozbor, M.A., *J. Organomet. Chem.*, 1987, vol. 326, p. 299.
70. Hamasaki, A., Kubo, K., Harashima, M., et al., *J. Phys. Chem. B*, 2021, vol. 125, p. 2987.
71. Yago, T., Tamaki, Y., Furube, A., and Katoh, R., *Crystal. Chem. Lett.*, 2007, vol. 36, p. 370.
72. Liu, H.B., Li, Y.L., Xiao, S.Q., et al., *J. Am. Chem. Soc.*, 2003, vol. 125, p. 10794.
73. Barashkov, N.N., Sakhno, T.V., Nurmukhametov, R.N., and Khakhel', O.A., *Usp. Khim.*, 1993, vol. 62, p. 579.
74. Ochi, J., Tanaka, K., and Chujo, Y., *Inorg. Chem.*, 2021, vol. 60, p. 8990.

Translated by Z. Svitanko